Journal of Colloid and Interface Science 505 (2017) 454–459

Contents lists available at ScienceDirect

Journal of Colloid and Interface Science

journal homepage: www.elsevier.com/locate/jcis

Regular Article

A building blocks strategy for preparing photocatalytically active anatase TiO_2/rutile SnO_2 heterostructures by hydrothermal annealing

Vagner Romito de Mendonça [a,*], Waldir Avansi Jr. [b], Raul Arenal [c,d], Caue Ribeiro [e]

[a] Instituto Federal de São Paulo – Câmpus Itapetininga, 18202-000 Itapetininga, SP, Brazil
[b] Departamento de Física, Universidade Federal de São Carlos, P.O. Box 676, CEP 13565-905 São Carlos, São Paulo, Brazil
[c] Laboratorio de Microscopias Avanzadas, Instituto de Nanociencia de Aragon (INA), Universidad de Zaragoza, Calle Mariano Esquillor, 50018 Zaragoza, Spain
[d] ARAID Foundation, 50018 Zaragoza, Spain
[e] Laboratório Nacional de Nanotecnologia aplicada ao Agronegócio – LNNA, Embrapa Instrumentação, 13560-970 São Carlos, SP, Brazil

GRAPHICAL ABSTRACT

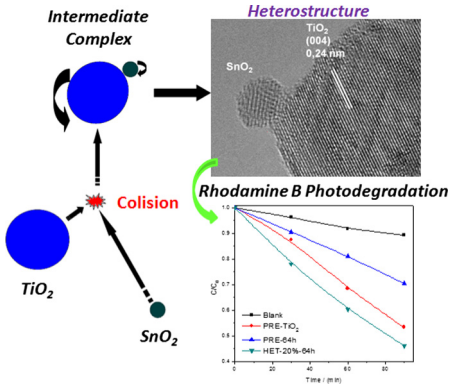

ARTICLE INFO

Article history:
Received 20 March 2017
Revised 5 June 2017
Accepted 7 June 2017
Available online 9 June 2017

Keywords:
Heterostructure
TiO_2
SnO_2
Oriented attachment
Photocatalysis

ABSTRACT

Effective heterostructures for photocatalysis need to present good electron-hole mobility among phases, a feature that is only attained with satisfactory interface quality. For very small sizes and with a stable colloidal state, the oriented attachment mechanism can be used to prepare suitable structures by means of a building blocks strategy, whereby preformed nanoparticles are used to control the desired amount of each phase in the heterostructure. Here, we show the success of this strategy for anatase TiO_2/rutile SnO_2 heterostructures, applying conventional hydrothermal annealing, where successive collisions among particles increase the probability of oriented attachment. The photodegradation of Rhodamine B in water under UV radiation was used as a probe reaction to evaluate formation of the heterostructure, as indicated by an increase in photoactivity. Increased heterostructure photoactivity was related to heterojunction formation and charge separation. The increased lifetimes of the photogenerated charges, due to heterojunction formation, enabled them to reach the oxides surface and promote photocatalytic reactions. The insights presented here may be used in a rationalized synthesis method to obtain heterostructures from preformed nanocrystals.

* Corresponding author at: Federal Institute of Education, Science and Technology of São Paulo, Av. João Olímpio de Oliveira, 1561, Itapetininga, SP CEP 18202-000, Brazil.
E-mail address: vrm@ifsp.edu.br (V.R. de Mendonça).

http://dx.doi.org/10.1016/j.jcis.2017.06.024
0021-9797/

1. Introduction

In recent years, a number of strategies have been developed aimed at improving the photocatalytic performance of semiconductors [1]. Among these, heterostructures have attracted much interest due to their promising properties, especially those related to the increase in the photogenerated charge lifetime [2]. This aspect is considered crucial in order to improve the photocatalytic performance of semiconductors [3]. Among the various semiconductors that have been studied, titanium dioxide (TiO_2), in the form of nanoparticles, aerogels, or thin films, has been employed to produce heterostructures in combination with different metals or metal oxides [4–9]. Among these materials, tin oxide (SnO_2) is of particular interest, because its electronic structure is perfectly matched to that of TiO_2, resulting in materials with superior photocatalytic properties [4,10,11].

Several studies have reported the growth, in reactive steps, of rutile SnO_2 over preformed anatase TiO_2 crystals [4,12,13]. In this procedure, the SnO_2 is formed directly over TiO_2 and epitaxial growth is expected. The arrangement in the interface depends on the synthesis parameters, such as the reagents concentrations and temperature. These factors influence characteristics including the coverage density and morphology of the materials, which directly affect photocatalytic performance [12,14]. However, it is difficult to control the simultaneous crystallization processes of two different components, or the modification of the surface of one crystalline material with another one, such as a semiconductor or a metal [13]. These difficulties could be overcome by the building of heterostructures using preformed nanoparticles with defined composition and properties as building blocks, although suitable technological procedures are still required to perform this process.

Previously, we proposed a kinetic model to describe the growth of heterostructures from preformed nanoparticles under microwave-driven hydrothermal conditions [15]. It was shown that the formation of heterojunctions was time-dependent and that the rate of hydroxyl radical formation under UV radiation should be directly related to the number of heterojunctions formed. In the proposed model, the rate of heterojunction formation could be described by:

$$\frac{d\left[(TiO_2/SnO_2)_{HS}\right]}{dt} = k \cdot [TiO_2][SnO_2], \quad (1)$$

where $(TiO_2/SnO_2)_{HS}$ represents heterojunctions. Since a diffusion-limited process was considered, the rate constant, k, could be described by:

$$k = \frac{2}{3}\frac{N_A k_B T}{\eta}\left(2 + \frac{R_{TiO_2}}{R_{SnO_2}} + \frac{R_{SnO_2}}{R_{TiO_2}}\right), \quad (2)$$

where N_A is Avogadro's constant, k_B is the Boltzmann constant, T is the annealing temperature, η is the coefficient of viscosity, and R is the radius of the nanoparticles.

This model was based on an interpretation of the oriented attachment mechanism, whereby particle growth occurs by directly attachment among locally oriented particles. In the colloidal state, the driving force is the particle boundary migration during effective collisions [16]. However, important points to consider are the faster kinetics of microwave-driven annealing, compared to conventional hydrothermal annealing, as well as the possible interference of electromagnetic fields in particle orientation [17].

In this work, we describe a photocatalytic study of TiO_2/SnO_2 heterostructures obtained by conventional hydrothermal annealing of preformed nanocrystals under different conditions. The main goal was to establish the relation between the hydrothermal conditions and photocatalytic performance, assuming that heterostructure formation was only affected by the rate of particle collisions [18]. TiO_2 and SnO_2 were considered suitable materials for use in this experiment due to their very low water solubility, so other crystal growth effects were not expected to occur [15]. The photoactivities of the heterostructures and pure TiO_2 were compared using the photodegradation of Rhodamine B (RhB) under UV radiation, before and after the hydrothermal treatments of the materials, as a probe of effective heterostructure formation. The results showed that oriented attachment should be considered in heterostructure formation, and that understanding of this mechanism could provide valuable insights for the technological production of these advanced materials.

2. Experimental section

The first step was the preparation of the TiO_2 and SnO_2 nanocrystals to be used as precursors for heterostructure formation. The oxides were synthesized according to the methods described by Ribeiro *et al.* [19] and Leite *et al.* [20], respectively, and were denoted PRE-TiO_2 and PRE-SnO_2.

For TiO_2, in a typical procedure, 250 mg of metallic Ti (99.7%, Aldrich) was added to 80 mL of a 3:1 H_2O_2/NH_3 solution (both 29.0%, Synth). After around 6 h, a transparent yellow solution was obtained, indicating formation of the $[Ti(OH)_3O_2]^-$ complex. In order to obtain the precursor, the solution of the complex was heated to boiling, followed by immersion in an ice-water cooling bath. After freeze drying, 200 mg of the resulting precipitate was re-dispersed in 100 mL of water, giving pH ~8,[21] and was submitted to hydrothermal treatment at 200 °C for 120 min in a controlled reactor, in order to crystallize the material. The product was collected after a freeze drying process in order to avoid further growth caused by application of heating for drying.

The synthesis of the SnO_2 nanoparticles was based on the hydrolysis reaction of tin(II) chloride dissolved in ethanol at room temperature, with slow addition of water resulting in the formation of crystalline nanoparticles at room temperature [20]. The chloride ions were removed by dialysis and the product was obtained after freeze drying. This synthesis method enabled the formation of particles with average size around 5 nm [22].

Heterostructures were prepared by the hydrothermal treatment of suspensions containing preformed nanocrystals of TiO_2 and SnO_2 in the desired proportions. Treatments were performed for different times at 200 °C in a controlled reactor. Hydrothermally treated PRE-TiO_2 was used as a reference. This step was performed in order to identify possible effects of the thermal treatment on the photoactivity of the materials, and the PRE-64 h sample was further analyzed in order to evaluate crystal stability after different treatment times. The samples were identified according to the oxides proportion and the hydrothermal treatment time. For example, the sample containing 20% by mass of SnO_2 and treated for 64 h was labeled HET-20%-64 h.

X-ray diffraction (XRD) analyses were carried out using a Shimadzu XRD 6000 X-ray diffractometer with radiation at 1.5456 Å, corresponding to the CuKα emission. The routine conditions used in these analyses were an exposure time of 1 s and an angular step of 0.02°. Crystallographic coherence lengths were calculated according to Scherrer's equation [23], deconvoluting each peak using a pseudo-Voigt approximation to determine the full width at half maximum (FWHM) value. The specific surface areas were determined by nitrogen physisorption at 77 K, which was measured using a Micromeritics ASAP 2020 instrument and evaluated by means of the standard BET procedure. The particle morphology and crystalline structure were characterized by conventional (TEM) and high-resolution (HRTEM) imaging using

an aberration-corrected FEI Titan-Cube microscope operated at 80 kV and equipped with a Cs corrector (CETCOR, from CEOS GmbH).

The surface-adsorbed hydroxyl groups on the TiO_2 photocatalyst samples were studied by Fourier transform infrared absorption spectroscopy (FTIR), using a PerkinElmer Spectrum 1000 instrument. The samples were mixed at a concentration of 0.3 wt% with potassium bromide (KBr), followed by pressing under 6 tons·cm^{-2} to obtain 100 mg pellets. Each pellet was analyzed using 50 scans at a resolution of 2 cm^{-1}. The samples were analyzed after drying at 110 °C for 24 h.

The photocatalytic activities of the samples for RhB oxidation were evaluated under UVC illumination. Different samples containing the same amount of photocatalyst were transferred to beakers and immersed in aqueous RhB solution (5.0 mg·L^{-1}). The beakers were placed in a photoreactor at a controlled temperature (20 °C) and illuminated by six UVC lamps (Philips TUV, 15 W, maximum intensity at 254 nm). Photocatalytic RhB oxidation was probed by UV–Vis measurements (Shimadzu UV-1601 PC spectrophotometer) after different periods of light exposure. Rhodamine B was chosen because degradation of this dye only depends on the photocatalyst parameters [24], so it was suitable for describing the photocatalytic properties of the synthesized materials.

3. Results and discussion

The as-synthesized preformed nanoparticles used in the heterostructure assembly were studied in detail previously [15,19,20]. As expected, PRE-TiO_2 and PRE-SnO_2 presented the XRD patterns indexed to the anatase (PDF#21-1272) and rutile (PDF#41-1445) crystalline phases, respectively.

The specific surface areas of PRE-TiO_2 and PRE-SnO_2 were 87.5 and 160 m^2·g^{-1}, as determined by N_2 adsorption analyses. Considering near-spherical shapes in both cases, the average sizes were around 18 and 5.5 nm, respectively [15]. The TEM images of the as-prepared nanoparticles indicated that PRE-TiO_2 had an average particle diameter of 20 nm, while PRE-SnO_2 presented a particle diameter of around 5 nm, in good agreement with the N_2 adsorption analyses for both oxides. The similarity of the diameter values obtained by different techniques for each oxide indicated that the samples were composed of almost monodispersed and deagglomerated nanocrystals. This was an important feature, because it reflected a constant particle cross-sectional area available for diffusion processes (as described in (Eq. (2))).

Fig. 1 shows the XRD patterns of the as-prepared samples. The XRD results confirmed that despite extended hydrothermal treatment, the PRE-64 h sample only contained the anatase TiO_2 phase. In the case of the heterostructured samples, less pronounced peaks related to the rutile SnO_2 phase were observed, which became more evident for the samples annealed for longer periods, indicating possible homostructure growth, also by oriented attachment. Since the hydrothermal treatment could induce crystal growth and affect the crystallinity of the materials, which are important factors in terms of photocatalytic performance, Scherrer's equation was employed to calculate the crystallographic coherence domains of the materials. The results showed no substantial differences among the materials, which all presented values of around 18 nm, even after hydrothermal treatment. It could therefore be concluded that since this kind of growth would affect crystallite sizes, there was no crystal growth due to Ostwald ripening induced by dissolution and precipitation of the materials, as expected for oxides with low solubility in water, such as TiO_2 and SnO_2.

Representative TEM images of the HET-20%-64 h sample are provided in Fig. 2. This sample was chosen because it showed more pronounced hetero- and homostructure growth, as predicted by

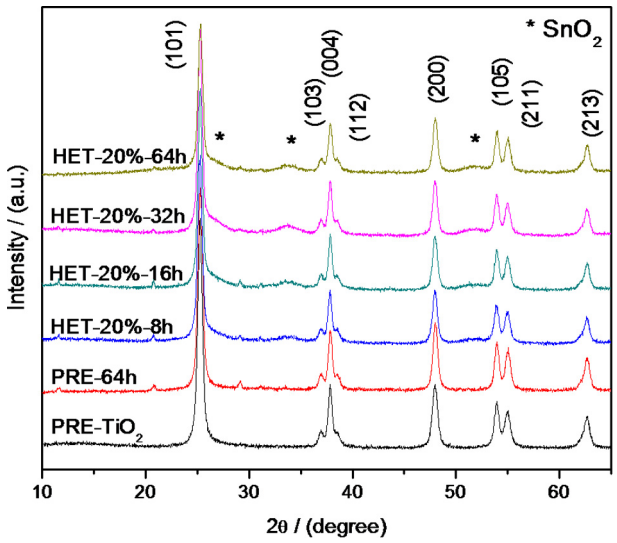

Fig. 1. XRD patterns for anatase TiO_2 and the anatase TiO_2/rutile SnO_2 heterostructures.

the kinetic model. Fig. 2(a) shows two distinct morphologies of non-uniformly dispersed nanoparticles, one type with size around 20 nm and another type with size around 5 nm. As shown in Fig. S1, TEM analyses of PRE-TiO_2 and PRE-SnO_2 indicated that these two morphologies could be attributed to TiO_2 and SnO_2 nanoparticles, respectively. The HRTEM analysis (Fig. 2(b)) and fast Fourier transform (FFT) analysis of region A confirmed that the ~5 nm nanoparticles corresponded to rutile SnO_2, while the ~20 nm nanoparticles were anatase TiO_2. The HRTEM micrograph (Fig. 2(b)) revealed an interesting feature, namely the attachment of SnO_2 nanoparticles to single TiO_2 nanoparticles and heterostructure growth. Another important point was the clear coalescence between SnO_2 nanoparticles (indicated by the red arrows in Fig. 2(b)), which reflected homostructure formation. This coalescence was unlikely to hinder heterostructure formation, but reduced the mobility of the SnO_2 nanoparticles. Fig. 2(c) shows an HRTEM image of a possible heterojunction formed between TiO_2 and SnO_2, where an interface between different oxides is clearly visible (indicated by the red arrow). Another interesting feature (Fig. 2(c)) was the inter[1]face formed between two TiO_2 particles (indicated by the yellow arrow). This effect could result in decreased photocatalytic performance, because such interfaces act as centers for photogenerated charge recombination [21]. It is more likely to occur during longer treatment times, which are therefore detrimental to the photocatalytic properties of these materials. The existence of TiO_2 or SnO_2 homostructures is envisaged in the adopted kinetic model.

Based on the TEM images, we can propose the occurrence of different reactions during the hydrothermal treatment. Considering the nanoparticles as molecules in chemical reactions, the possibilities are as follows:

$$TiO_2 + SnO_2 \rightarrow (TiO_2/SnO_2)_{HS} \quad (3)$$

$$TiO_2 + TiO_2 \rightarrow (TiO_2/TiO_2) \quad (4)$$

$$SnO_2 + SnO_2 \rightarrow (SnO_2/SnO_2) \quad (5)$$

$$2SnO_2 + 2(TiO_2/SnO_2)_{HS} \rightarrow (SnO_2/TiO_2/SnO_2)_{HS} + (TiO_2/SnO_2/SnO_2) \quad (6)$$

[1] For interpretation of color in Figs. 2, the reader is referred to the web version of this article.

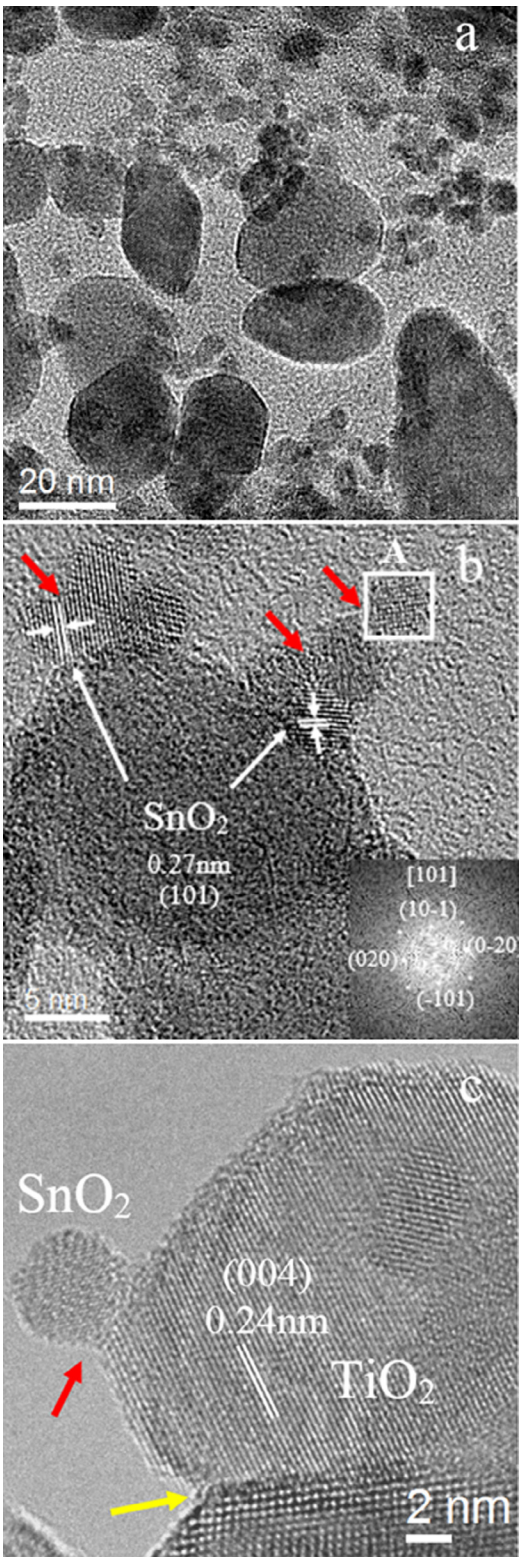

Fig. 2. TEM analysis of the HET-20%-64 h sample: (a) Low magnification TEM image showing dispersion of SnO_2 particles over TiO_2 particles. The oxides can be identified by their morphologies and sizes of ~5 nm and ~20 nm, respectively; (b) HRTEM image showing the possible points of heterojunctions between the two oxides. The coalescence of SnO_2 nanoparticles can be observed (red arrows), as predicted in the kinetic model. The inset shows fast Fourier transform (FFT) of region A; (c) HRTEM image showing coalescence between SnO_2 and TiO_2 nanoparticles (red arrow) and between two TiO_2 nanoparticles (yellow arrow). (For interpretation of the references to colour in this figure legend, the reader is referred to the web version of this article.)

$$TiO_2 + (TiO_2/SnO_2)_{HS} \rightarrow (TiO_2/TiO_2/SnO_2)_{HS} \quad (7)$$

In this set of equations, (Eq. (3)) represents the heterostructure formed by the collision between TiO_2 and SnO_2 nanoparticles. Several examples of this kind of structure can be seen in Fig. 2. Homostructure growth (represented by Eqs. (4) and (5)) can be clearly seen in Figs. 2(a) and (c). Due to the difference between the radii of TiO_2 and SnO_2 ($R_{TiO2} \approx 4\ R_{SnO2}$), the occurrence of heterostructure formation may not change the mobility of TiO_2 particles, making it possible that the reaction represented in (Eq. (6)) could occur. However, there are two possibilities for the attachment of SnO_2 nanoparticles over $(TiO_2/SnO_2)_{HS}$, as clearly shown in Fig. 2b. Firstly, a new heterojunction point could be formed: $(SnO_2/TiO_2/SnO_2)_{HS}$. Additionally, the attachment could proceed over another SnO_2 nanoparticle: $(TiO_2/SnO_2/SnO_2)$. A similar reaction could occur with TiO_2 nanoparticles, as presented in Eq. (7). However, a more likely possibility is the attachment of a TiO_2 nanoparticle with another TiO_2 nanoparticle: $(TiO_2/TiO_2/SnO_2)_{HS}$, as highlighted by the yellow arrow in Fig. 2(c).

It is important to point out that despite observation of clear interfaces between the particles, heterojunction formation cannot be confirmed solely by TEM analysis, since a heterojunction is characterized by the possibility of charge migration between the different semiconductors forming the heterostructure. Therefore, in order to study possible charge migration, and consequently heterostructure formation, photocatalytic experiments were performed to evaluate the performance of the as-prepared samples. The results for different as-prepared materials are presented in Figs. 3(a) and (b). Kinetic plots for the photocatalytic degradation of RhB using the different samples are shown in Fig. 3(a). All the processes followed pseudo-first order reaction kinetics [25]. The rate constants (k') obtained are presented in Table 1. The heterostructure samples obtained with hydrothermal annealing for between 8 and 32 h showed similar photoactivities, with better performance than PRE-TiO_2. The similarity between the performances of the heterostructures could be explained by the greater occurrence of coalescence events in the first stages of annealing, as predicted for homostructure growth by oriented attachment [18]. In a previous investigation of the capacity of TiO_2/SnO_2 heterostructures to produce hydroxyl radicals under UV radiation, it was shown that the production increased with hydrothermal treatment time, until reaching a plateau [15]. Since microwave heating was used in the earlier study, direct comparison of the effect of treatment time was not possible. However, the kinetic model proposed in the earlier work provided a good fit to the present data. Following heterojunction formation, there was no further modification of the interface during the treatment times investigated. In addition, considering that the samples were prepared using the same precursors and temperature, it could be concluded that the interface played the most important role in terms of the photoactivities of the samples.

The HET-20%-64 h sample showed lower photoactivity, compared to the other heterostructures with 20% SnO_2 (Fig. 3(b)). However, the photoactivity was higher than that of the PRE-64 h sample, which consisted of pure TiO_2 that had been treated during the same time. It is important to point out that the same behavior was observed for the samples treated during 32 h, with the heterostructure presenting higher photoactivity, compared to pure TiO_2 hydrothermally annealed during the same time (not shown). This demonstrated that the photocatalytic performance was not only due to the hydration effects that generally occur during hydrothermal treatment. In fact, the observed differences for the PRE-TiO_2, PRE-64 h, and heterostructure samples were indicative of the charge migration that is only possible after formation of heterojunctions between the oxides.

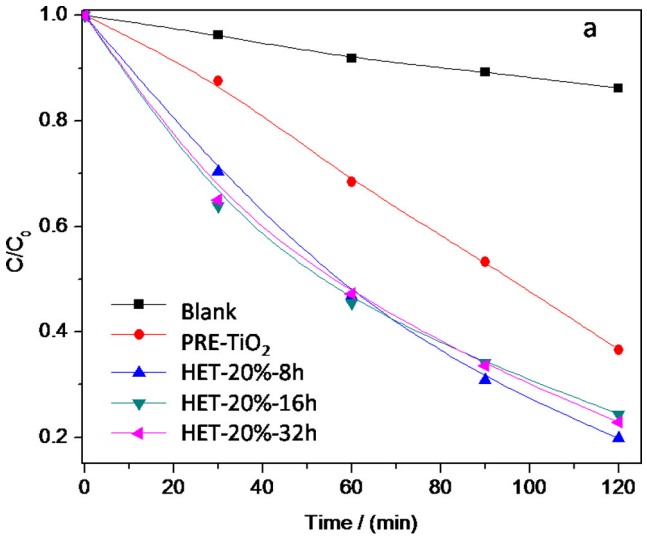

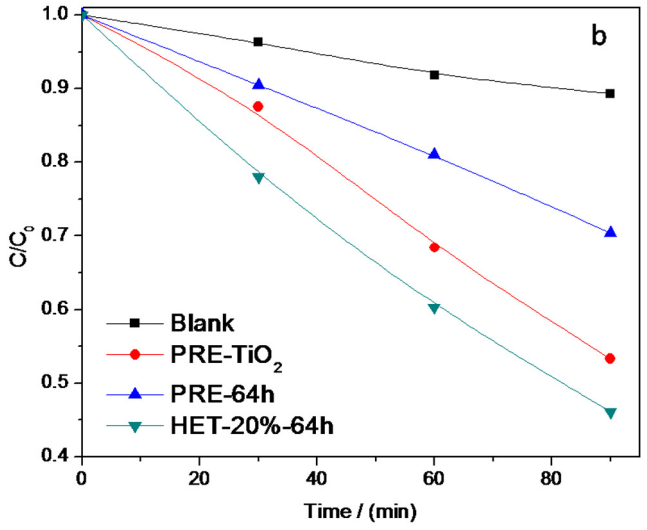

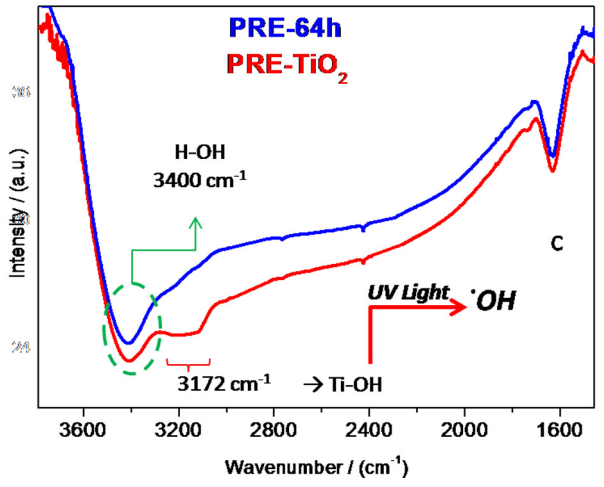

Fig. 3. (a) Kinetics of RhB photocatalytic degradation using PRE-TiO_2 and the synthesized heterostructures; (b) Kinetics of RhB photocatalytic degradation using hydrothermally treated TiO_2 and the heterostructure obtained after the same treatment time (64 h); (c) FTIR spectra of PRE-TiO_2 and PRE-64 h, highlighting the band related to the Ti-OH bond responsible for OH radical formation during UV irradiation.

Table 1
Pseudo-first order rate constants (k') for the as-synthesized samples, obtained from plots of $-\ln(C/C_0)$ *vs.* time. All the results showed $r^2 > 0.99$.

Sample	$k'/10^{-3}\cdot min^{-1}$
Blank	1.24
PRE-TiO_2	8.35
PRE-64 h	3.92
HET-20%-8 h	13.5
HET-20%-16 h	11.5
HET-20%-32 h	12.0
HET-20%-64 h	8.60

The FTIR analyses of the TiO_2 samples could be used to explain the lower photoactivity of the PRE-64 h sample, compared to the PRE-TiO_2 material. They could also be used to propose a hypothetical mechanism for RhB dye photodegradation under the conditions employed. Prior to the photocatalytic trials, suspensions of the photocatalysts in dye solution were kept in the dark for 24 h in order to measure the adsorption of the dye on the photocatalyst surface. No differences in the dye UV–Vis absorption were detected, indicating that there was no adsorption of the dye onto the photocatalysts. Since there was no significant adsorption, it could be considered that the main photodegradation pathway was the formation of oxidative species, mainly ·OH radicals [26], which were then responsible for oxidization and degradation of the dye, as shown in the following set of equations:

$$(TiO_2/SnO_2)_{HS} + h\nu \rightarrow e^-(SnO_2 \cdot CB) + h^+(TiO_2 \cdot VB) \quad (8)$$

$$h^+(TiO_2 \cdot VB) + OH^- \rightarrow {}^{\cdot}OH \quad (9)$$

$${}^{\cdot}OH + RhB \rightarrow \text{oxidization byproduct} \quad (10)$$

$$e^-(SnO_2CB) + O_2 \rightarrow {}^{\cdot-}O_2 \quad (11)$$

The first step is the photoexcitation of the semiconductor heterostructures and the formation of the electron/hole pairs. Due to the differences in the Fermi levels of the semiconductors, holes tend to agglomerate in the TiO_2 valence band: h^+ (TiO_2 VB), while electrons migrate to the SnO_2 conduction band: e^- (SnO_2 CB). Following various steps, h^+ (TiO_2 VB) are trapped by surface-linked hydroxyl groups, yielding ·OH, a strong oxidizing agent that can decompose organic dyes. It is important to highlight that for the occurrence of the reaction presented in (Eq. (9)), OH groups should be bound to the semiconductor surface, and not be only adsorbed [9,10,21]. Despite being widely proposed in the literature [10,27], the reaction presented in (Eq. 11), where electrons in the SnO_2 conduction band (CB) reduce molecular oxygen and produce superoxide anion radicals, does not lead to significant amounts of radicals, at least in standard conditions, since the reduction potential of its CB is insufficient for reducing O_2 ($E° = -0.33$ eV) [28].

Fig. 3(c) shows the FTIR spectra of the TiO_2 samples. Three main bands were observed in the spectral range employed: at 3400 cm^{-1}, related to stretching of adsorbed water; at 1635 cm^{-1}, due to angular deformation of water; and at 3172 cm^{-1}, corresponding to Ti-OH vibration. The intensity of the last band, for such diluted samples, was related to the quantity of hydroxyl groups attached to the TiO_2 surface [29]. It can be seen from the spectra that the precursor sample presented higher intensity at 3172 cm^{-1}. Since the photoactivity was related to ·OH radical formation, this sample presented higher photoactivity due to greater hydroxylation of the surface. Another important feature of the treated sample was crystal growth, as predicted by the model employed. The occurrence of coalescence and crystal

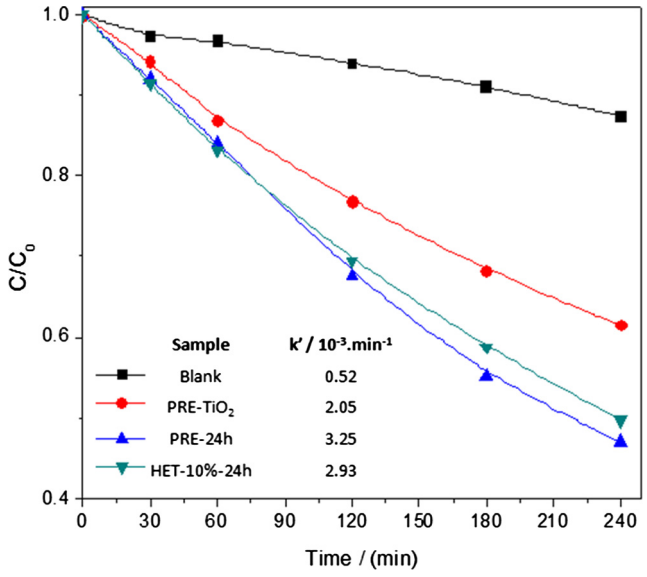

Fig. 4. Kinetics of RhB photocatalytic degradation using the PRE-TiO_2, PRE-24 h, and HET-10%-24 h materials.

growth in such a system can create recombination centers, hence decreasing the photoactivity [21].

Under the conditions applied in this work, especially regarding the ratio of the nanoparticle diameters, heterojunction formation was expected to be maximized when the mass ratio of SnO_2 was 20%, due to the optimized balance between the numbers of nanoparticles of each oxide, resulting in the highest ratio between hetero- and homojunction formation [15,21]. In order to confirm this, evaluation was made of the photocatalytic performance of $(TiO_2/SnO_2)_{HS}$ containing 10% (by mass) of SnO_2. The results are presented in Fig. 4. According to the kinetic model employed, the heterostructure formation rate should be lower for this ratio than in the first case. This was supported by the findings of the photocatalytic trials, since the HET-10%-24 h and PRE-24 h materials, which were both obtained using the same intermediate treatment time, showed almost the same photoactivity, as reflected by the *k'* values (Fig. 4 inset). Additionally, no difference was found between the rates of hydroxyl radical formation for TiO_2 and the heterostructure containing 10% SnO_2 obtained using microwave heating [15].

An important feature of the oriented attachment mechanism is that crystallographic defects generated during the growth process can be retained inside the structure [30]. Such defects were especially likely to occur in the present set of samples, due to the lattice mismatch between TiO_2 and SnO_2. As discussed before, this could negatively affect the photocatalysis, because the lattice defects could act as charge recombination centers, preventing the charge carriers from reaching the surface and promoting the photocatalytic process [21]. However, for the samples studied in this work, the difference in chemical potential generated by the Fermi level equilibration after heterostructure formation, which induced formation of a diffusion potential that acted as an electromotive force favoring electron injection [10], resulted in the charges passing through the interface, hence suppressing their recombination. This is the first time that the oriented attachment mechanism has been used to produce materials with high photoactivity.

4. Conclusions

This work provides information about the photocatalytic properties of TiO_2/SnO_2 heterostructures obtained from preformed nanocrystals used as building blocks in a hydrothermal annealing strategy. The heterostructures showed better performance in the photodegradation of RhB, compared to pristine TiO_2, which could be attributed to charge migration and a longer photogenerated charge lifetime. The synthesis process was relatively simple and could be explained based on the previously proposed kinetic model, hence contributing to the development of a predictable synthesis method for the preparation of metal oxide heterostructures.

Acknowledgements

The authors gratefully acknowledge the financial support provided by the Brazilian research funding agencies FAPESP and CNPq. The HRTEM analyses were conducted in the Laboratorio de Microscopias Avanzadas at the Instituto de Nanociencia de Aragon, Universidad de Zaragoza (Spain). Some of the research leading to these results received funding from the European Union Seventh Framework Program, under grant agreement 312483 ESTEEM2 (Integrated Infrastructure Initiative – I3). R.A. gratefully acknowledges support from the Spanish Ministry of Economy and Competitiveness (MINECO) through project grant MAT2016-79776-P (AEI/FEDER, UE) and from the Government of Aragon and the European Social Fund, under the project "Construyendo Europa desde Aragon" 2014–2020 (grant number E/26).

Appendix A. Supplementary material

Supplementary data associated with this article can be found, in the online version, at http://dx.doi.org/10.1016/j.jcis.2017.06.024.

References

[1] X. Li, J. Yu, M. Jaroniec, Chem. Soc. Rev. 45 (2016) 2603–2636.
[2] R. Marschall, Adv. Func. Mater. 24 (2014) 2421–2440.
[3] H. Wang, L. Zhang, Z. Chen, J. Hu, S. Li, Z. Wang, J. Liu, X. Wang, Chem. Soc. Rev. 43 (2014) 5234–5244.
[4] H.A.J.L. Mourão, W. Avansi, C. Ribeiro, Mater. Chem. Phys. 135 (2012) 524–532.
[5] I.A. Castro, W. Avansi, C. Ribeiro, CrystEngComm 16 (2014) 1514–1524.
[6] W.J. Zhou, G.J. Du, P.G. Hu, Y.Q. Yin, J.H. Li, J.H. Yu, G.C. Wang, J.X. Wang, H. Liu, J.Y. Wang, H. Zhang, J. Hazard. Mater. 197 (2011) 19–25.
[7] Y. Hu, D.Z. Li, Y. Zheng, W. Chen, Y.H. He, Y. Shao, X.Z. Fu, G.C. Xiao, Appl. Catal. B 104 (2011) 30–36.
[8] Y. Wang, J.W. Zhang, L.X. Liu, C.Q. Zhu, X.Q. Liu, Q. Su, Mater. Lett. 75 (2012) 95–98.
[9] F.J. Heiligtag, W. Cheng, V.R. de Mendonça, M.J. Süess, K. Hametner, D. Günther, C. Ribeiro, M. Niederberger, Chem. Mater. 26 (2014) 5576.
[10] C. Wang, C. Shao, X. Zhang, Y. Liu, Inorg. Chem. 48 (2009) 7261–7268.
[11] A. Marzec, M. Radecka, W. Maziarz, A. Kusior, Z. Pędzich, J. Eur. Ceram. Soc. 36 (2016) 2981–2989.
[12] J. Pan, S.M. Huhne, H. Shen, L.S. Xiao, P. Born, W. Mader, S. Mathur, J. Phys. Chem. C 115 (2011) 17265–17269.
[13] V.R. de Mendonça, O.F. Lopes, R. Fregonesi, T. Giraldi, C. Ribeiro, Appl. Surf. Sci. 298 (2014) 182–191.
[14] L. Shi, C. Li, H. Gu, D. Fang, Mater. Chem. Phys. 62 (2000) 62–67.
[15] V.R. de Mendonça, C.J. Dalmaschio, E.R. Leite, M. Niederberger, C.J. Ribeiro, Mater. Chem. A 3 (2015) 2216–2225.
[16] C.J. Dalmaschio, C. Ribeiro, E.R. Leite, Nanoscale 2 (2010) 2336–2345.
[17] M. Godinho, C. Ribeiro, E. Longo, E.R. Leite, CrystEngComm 8 (2008) 384–386.
[18] C. Ribeiro, E.J.H. Lee, E. Longo, E.R. Leite, ChemPhysChem 6 (2005) 690–696.
[19] C. Ribeiro, C.M. Barrado, E.R. Camargo, E. Longo, E.R. Leite, Chem-Eur. J. 15 (2009) 2217–2222.
[20] E.R. Leite, T.R. Giraldi, F.M. Pontes, E. Longo, A. Beltran, J. Andres, Appl. Phys. Lett. 83 (2003) 1566–1568.
[21] V.R. de Mendonça, C. Ribeiro, Appl. Catal. B-Environ. 105 (2011) 298–305.
[22] C. Ribeiro, E.J.H. Lee, T.R. Giraldi, E. Longo, J.A. Varela, E.R. Leite, J. Phys. Chem. B 108 (2004) 15612–15617.
[23] B.D. Cullity, S.R. Stock, Elements of X-ray Diffraction, Third ed., Addison-Wesley Publishing Company, Indiana, USA, 1967.
[24] H.A.J.L. Mourão, A.R. Malagutti, C. Ribeiro, Appl. Catal. A 382 (2010) 284–292.
[25] V.R. de Mendonça, H.A.J.L. Mourão, A.R. Malagutti, C. Ribeiro, Photochem. Photobiol. 90 (2014) 66–72.
[26] U.I. Gaya, A.H.J. Abdullah, Photochem. Photobiol. C 9 (2008) 1–12.
[27] A. Kar, S. Sain, D. Rossouw, B.R. Knappett, S.K. Pradhan, G.A. Botton, A.E.H. Wheatley, J. Alloys Compd. 698 (2017) 944–956.
[28] M. Grätzel, Nature 414 (2001) 338–344.
[29] (a) Z. Ding, G.Q. Lu, P.F. Greenfield, J. Phys. Chem. B 2000, 104, 4815-4820. b) J. Bertaux, F. Frohlich, P. Ildefonse, J. Sedimentary Res. 1998, 68, 440-447.
[30] S. Yin, F. Huang, J. Zhang, J. Zheng, Z. Lin, J. Phys. Chem. C 115 (2011) 10357–10364.